Talanta 213 (2020) 120813

Contents lists available at ScienceDirect

Talanta

journal homepage: www.elsevier.com/locate/talanta

TiO_2 nanoparticles and C-Nanofibers modified magnetic Fe_3O_4 nanospheres (TiO_2@Fe_3O_4@C–NF): A multifunctional hybrid material for magnetic solid-phase extraction of ibuprofen and photocatalytic degradation of drug molecules and azo dye

Erkan Yilmaz[a,b,c,d,*], Samaa Salem[a,b], Gokhan Sarp[a,b], Seda Aydin[a], Kubra Sahin[b], Ilknur Korkmaz[b], Donay Yuvali[a]

[a] Department of Analytical Chemistry, Faculty of Pharmacy, Erciyes University, Kayseri, Turkey
[b] ERNAM-Erciyes University Nanotechnology Application and Research Center, Kayseri, Turkey
[c] Technology Research & Application Center (TAUM), Erciyes University, Kayseri, Turkey
[d] Chemicamed Chemical Inc. Erciyes University Technology Development Zone, Kayseri, Turkey

ARTICLE INFO

Keywords:
Magnetic solid-phase extraction
Carbon nanofibers
Photocatalysis
Non-steroidal anti-inflammatory drugs
Antibiotics
Degradation
High-performance liquid chromatography
Analysis.

ABSTRACT

Accurate sensitive analysis of drug ingredient substances in biological, pharmaceutical and environmental samples and removal of drug ingredient substances in environmental samples owngreat importance for sustaining viability. The realization of these processes using a single material offers significant advantages in terms of cost, time and ease of use. In this study, TiO_2 nanoparticles and C-Nanofibers modified magnetic Fe_3O_4 nanospheres (TiO_2@Fe_3O_4@C-NFs) synthesized as a multifunctional material employing a simple hydrothermal synthesis method. This innovative material was exploited in the magnetic solid-phase extraction (MSPE) method for the preconcentration of ibuprofen and photocatalytic degradation of antibiotics, non-steroidal anti-inflammatory drugs (NSAIDs), and azo dye. To our knowledge, no studies have been previously conducted using the same material as magnetic solid-phase extraction adsorbent and magnetically separable photocatalyst. The characterization of TiO_2@Fe_3O_4@C-NFs was carried out by XRD, FE-SEM, EDX and Raman techniques. The main analytical parameters affecting MSPE performance of ibuprofen such as pH, sorbent amount eluent type and volume and sample volume were optimized. The optimum values of the method were determined at the following parameters: pH 4.0, adsorbent amount 150 mg and eluent 2 mL of acetone. Ibuprofen analysis after MSPE was carried out using a high-performance liquid chromatography diode array detection system (HPLC-DAD). The photocatalytic degradation efficiencies of TiO_2@Fe_3O_4@C–NF hybrid material for probe-analytes reached 80–100% and the complete degradation attained within the range of 8–125 min under UV irradiation. Simple preparation, practical isolation from solutions, high efficiency, reproducibility, and sustainability are the main advantages of the TiO_2@Fe_3O_4@C-NFs for MSPE and photocatalytic degradation applications.

1. Introduction

Over the past few decades, extensive concentration levels of pharmaceutical, personal healthcare and veterinary products including non-steroidal anti-inflammatory drugs (NSAIDs) and with varied groups of organic compounds found in the aquatic environment. This issue gained concerns because of the potential threats to aquatic life and human society [1–3]. Regards to the widespread usage of NSAIDs, these pharmaceuticals can easily subsist into the ground, surface and even drinking water resources because the adsorption coefficient of these compounds on the soil is low compared with their high polarity and hydrophilicity [4,5]. Ibuprofen is the most popular NSAIDs that can be applied to decrease rheumatic and chronic pains; it has a production volume of kilotons/year [6,7]. Unconscious consumption of ibuprofen, which is classified as endocrine disruptors, causes contamination of the aquatic environment depending on the discharge of domestic and industrial wastewaters [7].

Although researchers have strive considerable efforts in exploring the toxicity of pharmaceuticals and their transformation products, yet they have not been accepted as hazardous pollutants. It is necessary to

* Corresponding author. Erciyes University Faculty of Pharmacy, Department of Analytical Chemistry, 38050, Kayseri, Turkey.
E-mail address: erkanyilmaz@eriyes.edu.tr (E. Yilmaz).

https://doi.org/10.1016/j.talanta.2020.120813
Received 13 December 2019; Received in revised form 4 February 2020; Accepted 7 February 2020
Available online 08 February 2020
0039-9140/

validate a procedure for the analysis of ibuprofen's trace levels ($pg{\cdot}mL^{-1}$-$\mu g{\cdot}mL^{-1}$) in the environment. Biological samples with a complex and high level of interferences can be achieved by implementing an appropriate sample preparation method that concentrates and extracts the target analyte from the complicated matrices prior to instrumental analysis. The conventional analytical instruments are not still able to overcome complex sample matrices directly, and a smart one is less to be addressed [7–9]. Various analytical techniques have been utilized to determine ibuprofen in various biological and environmental media such as, UPLC [10], GC [11], HPLC [7], capillary electrophoresis [12], fluorescence spectroscopy [13], electrochemical methods [14]. Moreover, solid-phase extraction (SPE) and liquid-liquid extraction (LLE) methods are the most used sample pretreatment techniques to separate and preconcentrate ibuprofen from various samples [7,15–17]. Solid-phase extraction method has been extensively used for analyzing ibuprofen in biological samples like urine, bovine plasma, blood, human plasma, serum, food samples such as bovine milk, environmental samples like soil and sediments, water samples [7,15–17]. However, these conventional extraction procedures have some drawbacks including time- and price-consuming, using an excessive volume of toxic solvents and they also result in the loss of target analytes.

In recent decades, different nanomaterials have been utilized in progressive sample preparation methods because of their unique physical and chemical properties [18–20]. Nanomaterials have been integrated with sample pretreatment methods for enhancing the extraction efficiency of target analytes for a wide variety of samples. Among this nanomaterials, carbon nanotubes, graphene/graphene oxide, fullerenes, nanodiamonds, TiO_2, Al_2O_3, have been utilized as solid-phase extraction adsorbent for improving metabolite enrichment and analytical sensitivity [18–21]. Nanomaterials propose specific adsorption properties for widespread analytical and environmental applications owing to their small particle size, high surface/volume ratio and fast adsorption kinetic. In addition, nanoparticles have a large number of active groups on the surface that allow the interaction with organic and inorganic species. Plenty of researches have introduced nanomaterials with different chemical and morphological propertiesin this regard. In this context, carbon-based nanomaterials such as graphene (G)/graphene oxides (GO), carbon nanotubes (CNTs), fullerenes, carbon nanofibers (C-NFs) and nanodiamond (ND) are extensively used as qualified adsorbents in rapid advancing separation techniques [22,23]. Consisting of six-membered rings and delocalized electrons can ensure hydrophobic interactions with organic molecules. Not only π-π stacking is assigned for adsorption of organic molecules (e.g. drugs, enzymes, proteins, dyes, organic pollutants) but also hydrogen bonding, electrostatic and van der Waals forces are entrusted with bonding analytes on these nanomaterials. Carbon nanofibers are regarded as quasi-1-D carbon nanomaterials consiste of wrapped graphene layers into cylinders [24]. C-NFs are more useful in comparison with other carbonaceous nanomaterials for extraction processes because they have no leakage and aggregation problems in on-line systems [24].

Magnetic solid-phase extraction has been usually used as an innovative sample preparation method. With this in mind, the immobilization of magnetite (Fe_3O_4) and hematite (Fe_2O_3) nanoparticles on other solid phase extraction nano-sorbents facilitate and accelerate the phase separation step by using an external magnet without requiring no centrifugation or filtration [7,25]. Adding magnetic nanoparticles improves the extraction properties of sorbents and minimizes the adsorbent losses [7,25]. It is also worth to mention that the adsorption and determination of pharmaceuticals are highly significant during the purification of the aforementioned drugs enabling heterogeneous catalytic degradation such as TiO_2 nanoparticles (TiO_2 NPs). Therein, the usage of TiO_2 for photocatalytic degradation of pharmaceutical hazardous components has attracted a great concern on account of its high photocatalytic performance, low cost, environmental friendliness and chemically and physically inertness [26–28]. Moreover, to improve the photocatalytic activity of carbon-based nanomaterials, modifications with photocatalytic active nanoparticles such as TiO_2, ZnO and Bi_2WO_6 is an effective strategy [27,29,30]. However, it is impractical to recover these nanomaterials from liquid samples after the process is completed. Hence, many investigations have been performed by modifying the interlayer and outer layer of TiO_2 NPs with magnetic Fe_3O_4 nanoparticles [31–33].

In order to reveal the multifunctional property of a material, in this study, a new material was designed to be used both in magnetic solid phase extraction of trace level ibuprofen and photocatalytic removal of organic pollutants in water. For this purpose, we used TiO_2 nanoparticles and C-Nanofibers modified magnetic Fe_3O_4 nanospheres (TiO_2@Fe_3O_4@C–NF) for the magnetic solid-phase extraction of ibuprofen in biological, pharmaceutical and environmental water samples prior to the analysis that carried out by HPLC-DAD and photocatalytic degradation of antibiotics, NSAIDs and azo dye. We took advantage of the synergetic effect of TiO_2@Fe_3O_4@C–NF hybrid nanomaterial comprised between the adsorption of target molecule and the photocatalytic degradation on nano TiO_2.

2. Experimental

2.1. Materials and reagents

Analytical grade reagents were used throughout the experimental study. TiO_2 nanoparticles had a particle size of 21 nm, C-nanofibers possessed a diameter of 100 nm and 20–200 μm of length, $FeCI_3$, $NaCH_3COO$ and ethylene glycol were obtained from Sigma Aldrich (ST Louis, USA). All solvents were for chromatographically analyzed employingHPLC grade and purchased from SigmaAldrich (St. Louis, MO, USA). Milli-Q system deionized water system (Millipore, USA) was used to obtain deionized water (Resistivity 18.2 MΩ cm).

2.2. Equipment

The analysis of drugs was performed by the HPLC-DAD system including (C18) column (150 × 4.6 mm, 5 μm particle size and 25 °C column temperature, USEM research, and development company, Turkey). The assessment of methylene blue dye removal was acquired by a UV-VIS spectrophotometer. Acetonitrile: methanol (50:50 v/v) mobile phase at a flow rate of 1.2 mL min^{-1} was used. UV detection after chromatographic separation was effectuated at different absorption maxima depending on the used probe-analyte. A photocatalytic reactor with 400 W power of UV-lamp (Unitermrm, Turkey) was employed for the photocatalytic degradation experiments. The structure and morphology of the synthesized Fe_3O_4@C-NFs and TiO_2@Fe_3O_4@C-NFs hybrid nanomaterial were investigated by field emission scanning electron microscope (FE-SEM, Gemini 550). The crystallographic structures of Fe_3O_4 nanoparticles and TiO_2@Fe_3O_4@C-NFs hybrid nanomaterial were illuminated by employing Bruker AXS D8 X-ray powder diffractometer with simple cubic lattice and CU Kα radiation (λ = 0.15406 nm), and the scan range (2θ) was from 5° to 90°. Raman spectrums of TiO_2, Fe_3O_4 nanoparticles, and TiO_2@Fe_3O_4@C-NFs hybrid nanomaterial were recorded by enabling WITec alpha 300 M dispersive Raman spectrometer consisting He–Ne laser system (Excitation of wavelength is 532 nm).

2.3. Preparation of TiO_2@Fe_3O_4@C–NF hybrid nanomaterial

The spherical magnetic nanoparticles (Fe_3O_4 NPs) utilized in this study were synthesized by facile, one-step hydrothermal method. 1.0 g of $FeCI_3$ and 4.0 g of $NaCH_3COO$ was dissolved in 50 mL ethylene glycol. The solution was placed in an ultrasonic bath for 15 min. Thereafter, the solution was transferred into a Teflon-lined stainless steel hydrothermal unit and the oven was heated up and its temperature was maintained at 180 °C for 8 h. After the hydrothermal process

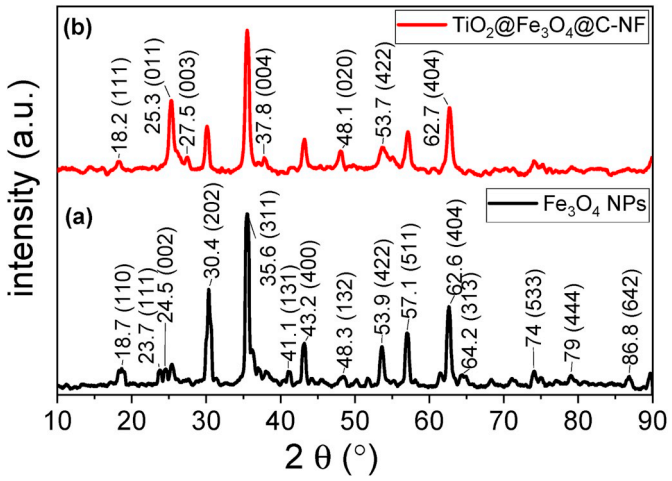

Fig. 1. XRD diffraction pattern of the prepared nanocomposites (a) Fe_3O_4 and (b) TiO_2@Fe_3O_4@C–NF. 2θ (degree) and Miller indices are also depicted on the diffraction pattern. Powder x-ray diffraction equipped with a copper X-ray source and emits X-ray radiation wavelength, λ = 1.5406 Å.

elapsed and the usage unit was cooled, then Fe_3O_4 NPs were washed two times with deionized water and acetone and subsequently they were further dried overtime in an oven at 80 °C.

To establish efficient surface-modified hybrid nanomaterials that carry enhanced photocatalytic and adsorption properties,s surface-functionalized spherical-like Fe_3O_4 NPs, using both as-synthesized TiO_2 NPs and C-NFs, has been fabricated. For this purpose, 0.1 g of TiO_2, 0.5 g of C–NF and 0.5 g of Fe_3O_4 were weighed and homogeneously dispersed in 25 mL of EG by ultrasonic bath for 1 h. The obtained mixture was transferred into a Teflon-lined stainless steel hydrothermal unit. Afterwards, the hydrothermal unit was positioned in the oven at 180 °C for 12 h. After the hydrothermal unit was cooled, TiO_2@Fe_3O_4@C–NF hybrid nanomaterial was washed two times with ultrapure water and acetone. The last product was dried in an oven at 80 °C. The synthesis procedure is illustrated in Fig. 1.

2.4. Photocatalytic degradation of drugs and azo dye

Photocatalysis performance of TiO_2@Fe_3O_4@C–NF hybrid nanomaterial was assessed in 100 mL of model solution medium including a known concentration of each of drugs or azo dye. For this purpose, 100 mg of TiO_2@Fe_3O_4@C–NF was added into 150 mL of model solution and the mixture was stirred in a well-closed and dark chamber until adsorption of organic molecule completed. Posteriorly, the mixture was transferred to the photocatalytic reactor and subjected to 400 W of UV-halogen-lamp, which located at the center of the reactor. The photocatalytic degradation ratio of each of the drugs or azo dye was investigated over 200 min. In order to detect the rate of photocatalytic degradation against time, aliquots of 1.0 mL of sample were withdrawn for analysis at scheduled time intervals (10 min/sample) to be analyzed using either HPLC or UV-VIS spectrometer. The degradation rate of each molecule was determined by exploring the change of intensity of the peak of analyte against time in the spectra recorded utilizing HPLC or UV-VIS spectrometer.

2.5. Magnetic solid-phase extraction

A model solution of 15 mL was prepared in phosphate buffer medium (10 mM pH 4.0). The solution including a known concentration of ibuprofen was placed into a 50 mL centrifuge tube and 150 mg of TiO_2@Fe_3O_4@C–NF hybrid nanomaterial was added. In order to adsorb ibuprofen molecules on the TiO_2@Fe_3O_4@C–NF hybrid nanomaterial, the nanoparticles were dispersed with the help of a vortex for 5 min. Finally, the TiO_2@Fe_3O_4@C-NFs were isolated from the sample solution by applying an external magnetic field. The resultant phase was totally removed. Next, TiO_2@Fe_3O_4@C–NFs were dispersed into 2.0 mL of acetone and vortexed for 5 min to elute ibuprofen molecules. In the last stage, the eluent phase was taken by using a micropipette, filtered through a 0.22 filter and analyzed with the HPLC-DAD detection system. For the next MSPE process, the TiO_2@Fe_3O_4@C–NFs hybrid nanomaterial was washed with water. The same MSPE/HPLC-DAD procedure was applied to standard solutions and blank samples.

2.6. Applying the MSPE method for some field measurements

We applied the MSPE method to the surface water samples that were collected from different regions of Turkey; wastewater from factory region in Kayseri City-Turkey, lake water from Van City-Turkey and seawater from Antalya City-Turkey. Before applying the MSPE, the collected surface water samples were filtered utilizing a 0.45 μm membrane filter. The application of the developed MSPE method was probed using pharmaceutical samples. For this application, 10 tablets from the same drug sample were taken and ground to reach homogenized 65 mesh of particle size. The homogenized drug samples (5.0 mg) were dissolved in 100 mL of methanol by being placed in an ultrasonic bath and irradiated for 20 min. irradiation. Known volume from the methanol phase was taken, mixed with water and pH of sample solution was adjusted to 4.0 prior to the MSPE method. For the syrup drug samples, 50 μL from syrup samples were diluted to exact volume with water, the pH of the sample solution was adjusted to 4.0 and further subjected to the MSPE method. We also applied our method to reference urine sample obtained as commercial.

3. Results and discussion

3.1. Characterization of TiO_2@Fe_3O_4@C–NF

The X-ray patterns of magnetic nanoparticles (MNPs) and TiO_2@Fe_3O_4@C–NF are shown in Fig. 1. The matched phases and quantities (%) were calculated using Match 3! Software. Herein, the chemical constituents contributed to synthesize ferric oxide impregnated titanium dioxide and carbon nanofibers (TiO_2@Fe_3O_4@C–NF) that was assigned as Fe_3O_4 (Magnetite), Fe_2O_3 (hematite), TiO_2 (Anatase) and amorphous carbon nanofibers (hexagonal graphite structure) with percentage quantities of 30.1, 14.8, 13, 42.1%, respectively. Change in d-spacing was observed along with the diffraction pattern due to the structural changes, where the lattice planes gave rise to the smallest Bragg angle had the largest d-spacing. The characteristic diffraction peaks and lattice planes for the simple cubic lattice of Fe_3O_4 assigned at 18.2° (111), 30.1° (202), 35.5° (131), 43.2° (040), 53.7° (242), 57.1° (151), 62.7° (404), 74° (353), 86.8° (624) were clearly observed. Additionally, the diffraction peak and the lattice planes corresponding to TiO_2 were assigned at 25.3° (011), 27.5° (003), 37.8° (004), 48.1°(020).

However, as shown in Fig. 1 that the predominant diffraction peak of TiO_2 was assigned at 25.3°; this plane is very close to the peak of C-NFs, 26° (002). As a result, this could explain the overlapping of both peaks for TiO_2 and C-NFs in the samples containing both constituents; obstructing the visualization of carbon peak and its relevant plane [56]. It is also assumed that the disappearance of the C-NFs second diffraction peak at 43.4° maybe attributed to more than one reason in our case: (**i**) it's overlapping with one of Fe_3O_4 diffraction peak (**ii**) the formation of a homogeneous coating of TiO_2 on C-NFs (**iii**) less aggregated pores the synthesized nanocomposite catalyst. At the interface between XRD diffraction peaks; it was observed that the intensity of the predominant peak of Fe_3O_4 has been alleviated, this implied the influence of TiO_2 on the crystallinity of Fe_3O_4. Moreover, the absence of extra peaks in the photocatalyst XRD diffraction pattern suggested that no chemical reaction accomplished between Fe_3O_4 and TiO_2 in the non-thermal mechanism. Furthermore, the percentage of crystallinity calculated for

TiO_2@Fe_3O_4@C-NFs nanocomposites photocatalyst via Eq. (1) was ~81%.

The percentage of crystallinity was calculated according to the following Eq. (1):

$$\text{Crystallinity} = \frac{\text{Area of crystalline peak}}{\text{Area of all peaks (crystalline + Amorphous)}} \times 100 \quad (1)$$

Furthermore, the average crystallite size of the prominent diffraction peaks was calculated via Debye Scherrer formula (Eq. (2)). The calculated average crystallite size for diffraction peaks of TiO_2@Fe_3O_4@C–NF nanocatalyst was estimated to be ~23.1 nm.

$$\beta\ (2\theta) = \frac{K\lambda}{L\cos\theta} \quad (2)$$

where, β_{hkl} is the crystallite size perpendicular to the normal line of the (hkl) plane, which is the full width at half maximum (FWHM) of the hkl diffraction peak in radian, K grain shape factor (~0.89), hkl is the Bragg angle of the hkl peak and X-ray wavelength, θ is the Bragg diffraction angle of the 2θ peak; λ = 1.5406 Å. Moreover, β_{hkl} is the peak width that is inversely proportional to the crystallite size (L).

Raman spectroscopy was employed to investigate more about the synthesized nanocatalyst structural, chemical and vibrational bands. Fig. 2 shows that Raman spectrum and the bulk structure of (a) TiO_2 NPs (anatase phase) (b) Fe_3O_4 NPs (c) TiO_2@Fe_3O_4@C-NFs. Anatase phase of TiO_2 has six Raman active modes ($1A_{1g} + 2B_{1g} + 3E_g$); clearly

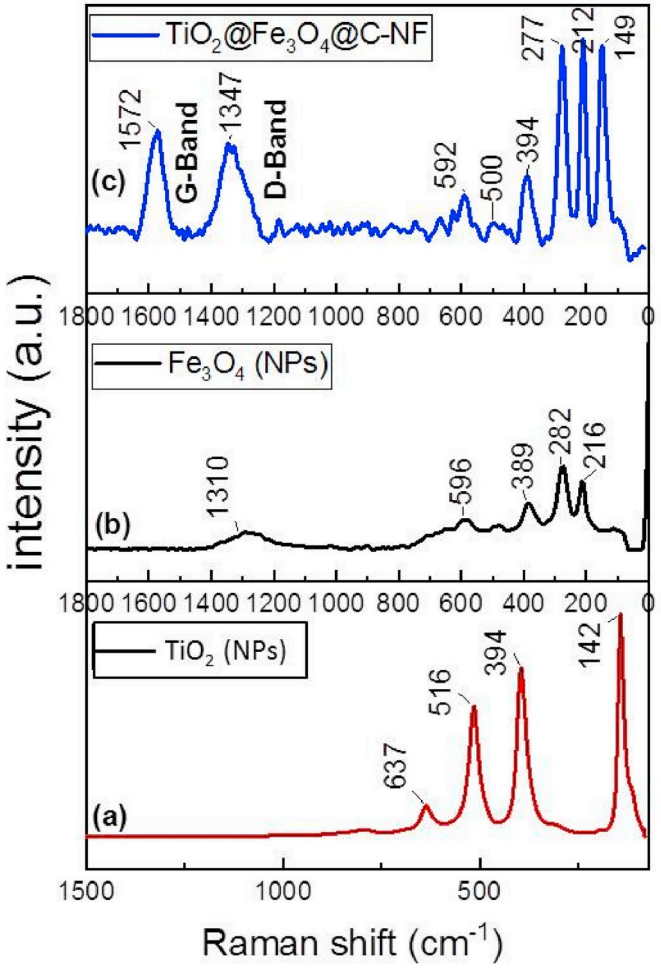

Fig. 2. Raman spectrum of (a) TiO_2 anatase phase (b) Fe_3O_4 and (c) TiO_2@Fe_3O_4@C-NFs; D and G band of carbon nanofibers are depicted in the figure inset. The utilized laser beam was with excitation wavelength ~532 nm.

determined in Raman spectrum and assigned at the following Raman frequencies (cm^{-1}): 142 main band at (E_g)* mode, 197 (E_g), 394 (B_{1g})*, 513 (A_{1g}), 516 (B_{1g})*, 637 (E_g)* [34]. The asterisk identifies the stronger vibrational frequencies in the Raman spectrum collected at room temperature (Fig. **2**). In Fig. 2**c**, the two large symmetrical broad bands ascribed to the D-band and the G-band of crystalline graphitized carbon were determined around 1347 and 1576 cm^{-1}, respectively. They are attributed to the disordered carbon of the in-plane vibrations within a structured defect (D band) and graphitic stretching mode of sp^2 carbon (G band). The small shifted peaks corresponding to TiO_2 and assigned at 149 (E_g), 394 (B_{1g}) cm^{-1} presume about the presence of the untransformed anatase phase of TiO_2. Moreover, the sharp peaks at Raman frequencies at 211 and 277 cm^{-1} are corresponding to Fe_3O_4. It is assumed from (Fig. 2) that all sharp peaks ascribed for Fe_3O_4 and presented in (Fig. 2b) confronted a small shift due to being overlapped with the closer TiO_2 bands revealing a new shifted bands illustrated in the inset of Fig. 2c.

The morphology of as-synthesized TiO_2@Fe_3O_4@C–NF nanomaterial was depicted by using field emission scanning electron microscope (FE-SEM) technique (Fig. 3). Fig. 3A displays the SEM image of Fe_3O_4 nanospheres in which nearly smooth monodispersed well-structured spheres with an average size distribution of 0.25 μm and standard deviation 0.4 were determined by the statistical Image J software. However, some smooth colloidal Fe_3O_4 agglomerations were also observed (Fig 3). TiO_2 NPs were determined sometimes as denes agglomerates with a rough surface the distributed homogeneously on the surface of the nanocatalyst. After the addition of TiO_2 NPs, with average particle size ~14 nm and standard deviation 0.1; to the unformal Fe_3O_4 nanosphere, a superficially rough surface was discerned (Fig. 3B). The micrographs (with bar scale 1 μm) confirmed the presence of well-preserved uniform and smooth carbon fibers meter distribution ~ 80 nm and standard deviation 0.06 (Fig. 3C). TiO_2 NPs decorated C-NFs and rough beads were randomly observed on the surface of C-NFs, this may imply the production of TiO_2@Fe_3O_4@C–NF nanocomposite, where it is assumed that the structure was comprised of carbon nanofiber embedded TiO_2 nanocrystals.

FT-IR spectrums of TiO_2 NPs and TiO_2@Fe_3O_4@C–NF nanomaterial are shown in Supplementary Fig. 1. Vibration peak for Ti–O bond is seen at 1393 cm^{-1}. The vibration peaks for Ti–O–Ti band and O–Ti–O band are seen between 400 and 1300 cm^{-1} respectively. A new peak around 531 cm^{-1} corresponds to Fe–O vibration. TGA analysis for the TiO_2@Fe_3O_4@C–NF nanomaterial was carried out (Supplementary Fig. 2). As a result of the heat treatment applied up to 150 °C, it is seen that there is a decrease of 32% in the mass due to the removal of the moisture in the TiO_2@Fe_3O_4@C–NF nanomaterial and there is no loss in the mass since there is no chemical change in the components in the TiO_2@Fe_3O_4@C–NF nanomaterial when the higher temperatures are reached.

3.2. Photocatalytic activities and kinetic study of TiO_2@Fe_3O_4@C–NF

3.2.1. Photocatalytic degradation of drugs molecules

The photodegradation of non-steroidal anti-inflammatory drugs (paracetamol and dexketoprofen) and antibiotics (trimethoprim and sulfaguanidine) was monitored exploiting HPLC device. The kinetics of the photocatalytic degradation rate of the probe molecules were adopted according to the Langmuir-Hinshelwood kinetics model as given in the following (Eq. (3)):

$$\ln\left(\frac{C_x}{C_0}\right) = -Kt + \text{constant} \quad (3)$$

Where; K (min^{-1}) is the pseudo-first-order rate constant or photocatalyst rate of deposition; it was calculated from the slope of ln (C_x/C_0) as a function of irradiation time t. This law is based on the fact that the rate of the reaction increases proportionally with the rate of decay of the reactant. If Eq. (3) is compared with the equation of straight-line, a

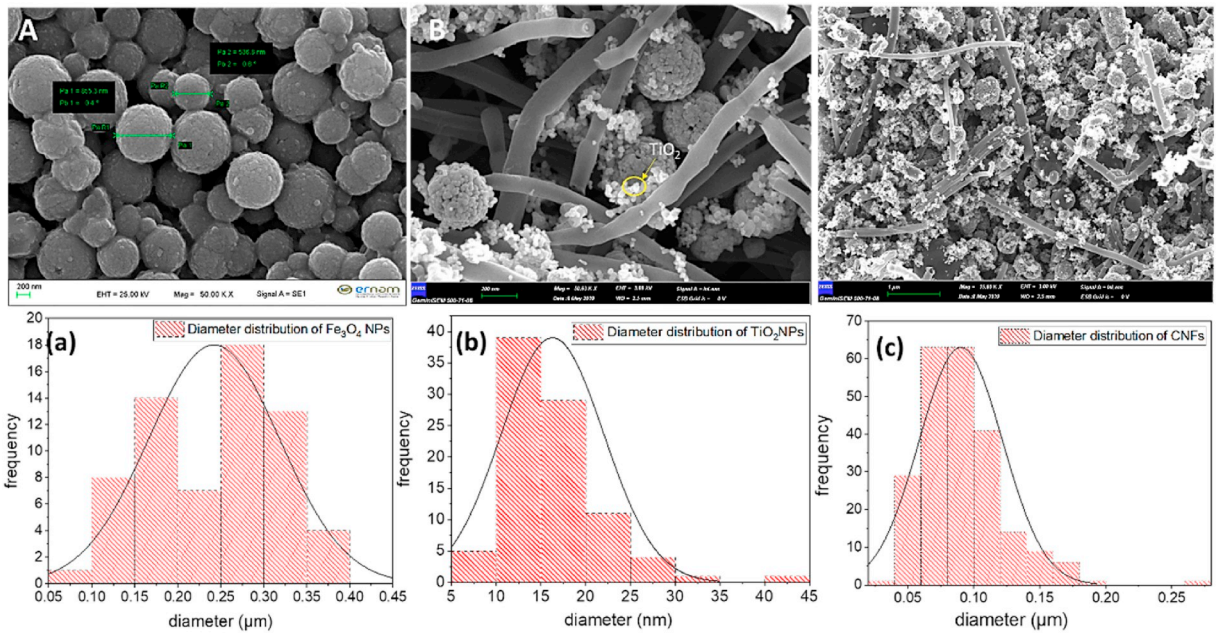

Fig. 3. SEM images (A) Fe_3O_4 magnetic nanoparticles (B, C) as-synthesized TiO_2@Fe_3O_4 @C–NF. The scale bar represented in the inset of the SEM images. The histogram for the average particle distribution for (a) Fe_3O_4 NPs (b) TiO_2 NPs (c) C-NFs is depicted in the inset of the figure. Statistical analysis and average particle size distribution were performed using ImageJ software. Both particle diameter and standard deviation for > 400 measurements were calculated.

plot of ln [C_x] versus t should give a straight line whose slope is - K and intercept of the plot is ln [C_0]. Rate constant can be utilized in comparing the rate of different reactions and define the capacity of the photocatalyst to adsorb the probe analytes.

The HPLC analysis was conducted over a period of 200 min for all the probe drug molecules and never stop the running experiment until reaching the climax and the plateau stage. The HPLC chromatogram showed the variations in the area under the resultant characteristic peak for probe-analytes over a specific time of irradiation. The results showed that the concentration of the probe-analytes and their characteristic peak intensity decreased with the increase of the irradiation time. This means that the basic structure was devastated along with the photodegradation reaction. The kinetics plot ln (C_x/C_0), constant K (min^{-1}) and corresponding correlation constants are demonstrated in (Fig. 4). All the calculated regression values for the probe-analytes were closed to unity gave proof that the photocatalysis followed the pseudo-first-order kinetics. Temporally, the concentration of all the probe-analytes exhibited a declination trend and attained a degradation and removal (80–100%) over a time interval from 100 to 125 min (Fig. 4). In fact, the photodegradation processes strongly depend on the existence or the lack of molecular oxygen as well as the nature of the probe-analytes chromophores [35]. Consequently, when UV light hits, the chromophore can thus be absorbed by exciting an electron from its ground state to the excited energy level; this causes what so-called photoinduced degradation and the generation of reactive oxygen species. In this context, the rate of decay and kinetics plot for dexketoprofen recorded the highest photosensitivity. However, sulfaguanidine recorded the highest photostability and the lowest rate of degradation and deposition rate of constant. Heterogeneous photocatalysis and the recorded rate of degradation and rate of phototransformation depend on the relevant chemical nature (organic or inorganic) and chromophores of the used probe-drug molecule (Supplementary Table 1). Ketoprofen, 2-(3-benzoylphenyl)-propionic acid, is a non-steroidal anti-inflammatory drug (NSAIDs); it is widely used for the medication of rheumatoid arthritis, osteoarthritis, ankylosing spondylitis, in addition to non-rheumatoid diseases/postoperative pain. It poses a threat to human beings and the ecological system because their polar-non-volatile nature avoids them from escaping out of the aquatic system. Dexketoprofen (DKP) contains photochemical stable benzophenone as a chromophore; it illustrates uncommon chemistry for benzophenone substitution. The rapid direct photolysis of ketoprofen under UV-lamp irradiation (4000 W/m^2, 290 nm < λ < 700 nm) was attributed to the fact that the carbonyl moiety is in conjugation with two aromatic rings. When the carbonyl is highly conjugated, the energy of the n-π* transition is lowered, resulting in a very reactive triplet state [36]. Due to the existence of the carboxylic group (aqueous pK_a ca. 4.7) [67, 68], DKP may exist as the neutral form or as the anion KP^-; depending on the pH of the medium. Prior to the irradiation with ≥380 nm neutral DKP acts as a conventional benzophenone owing to the high efficiency of intersystem crossing to form an excited triplet (^{3}KP), while KP^- decarboxylates.

In the case of the highest photostability sulfaguanidine drug molecule, these sulfonamide structures contain an aromatic ring, heteroatoms and other functional chromophore groups (Supplementary-Table 1), which are rapidly affected when exposed to UV-irradiation. Zessel et al. have investigated the tendency of sulfonamides degradation under the impact of natural and artificial UV-radiation [37]. They reported that sulfonamides undergo relatively slow photodegradation and it was most pronounced after the irradiating sulfonamides with combined radiation from UVA and UVB radiation, then after the UVA radiation and ultimately following the subjection to sunlight. The degradation rates of various sulfonamides; under the same conditions, were different. They reported that different sulfonamide structure was used and their parent structure was almost removed with rate ranged between 4 hand 7 days; after being subjected to the combined UVA/UVB radiation. Thus, one can assume that the tendency to photodegradation depends on the chemical structure of sulfonamides. In our case and by enabling TiO_2@Fe_3O_4@C–NF photocatalyst; it was able to complete the degradation of sulfaguanidine within ~90 min. Although trimethoprim is from the same family of sulfaguanidine, its rate of degradation came in the second place after dexketoprofen and it was utmostly removed within ~125 min. This may be attributed to the stereochemical configurations of trimethoprim that may be more suitable to chelate with the surface of TiO_2@Fe_3O_4@C–NF photocatalyst than sulfaguanidine. (Supplementary- Table 1). The rate of degradation (~125 min) of paracetamol came at third place among the used probe-

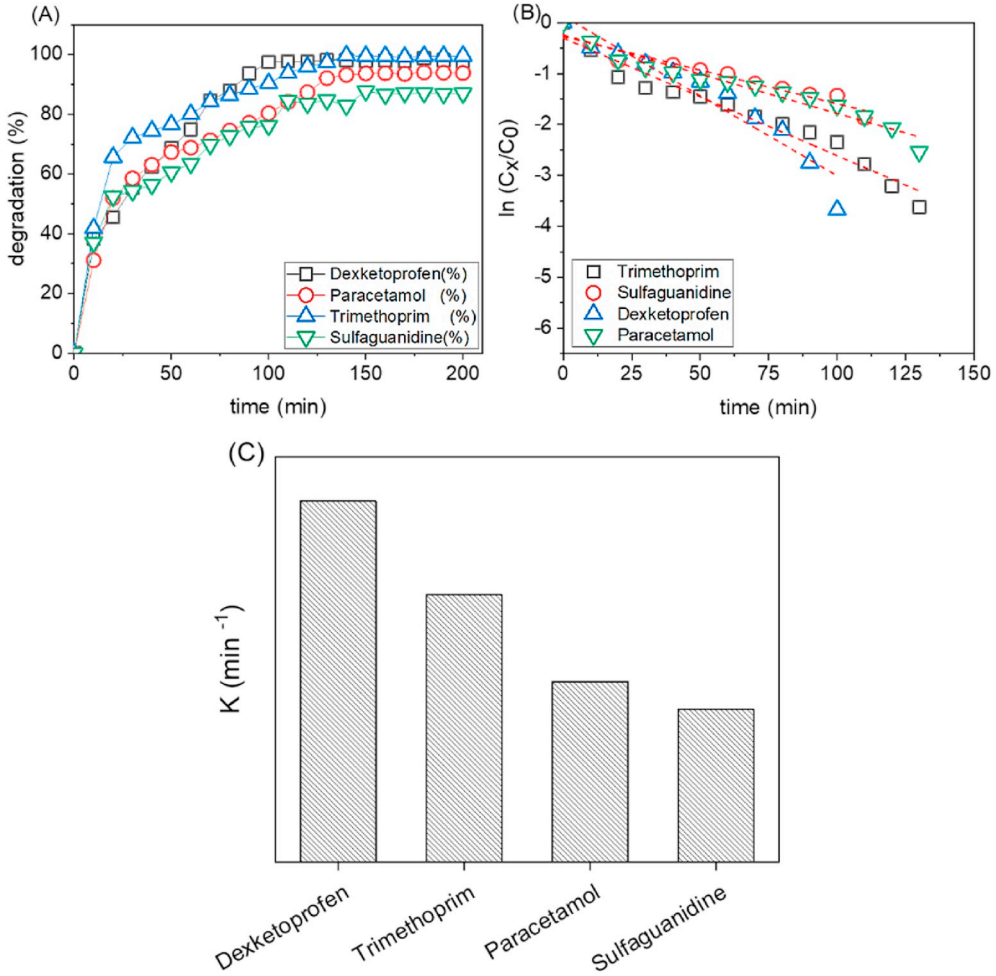

Fig. 4. (A) HPLC chromatography showing the degradation rate and the kinetics of the photocatalytic degradation rate for dexketoprofen, trimethoprim, paracetamol, and sulfaguanidine (B) The kinetic plot (ln C_x/C_0) of the photocatalytic degradation rate of the probe-analytes and (C) Pseudo-first-order rate constant K (min^{-1}) values (photocatalyst rate of deposition) for different drug molecules. Different symbols are used relevant to different drugs of similar concentration (5 ppm) depicted in the figure inset. The concentration of photocatalyst (0.67 mg ml^{-1}).

drug molecules. Paracetamol (acetaminophen), with chromophores procaine and phenolphthalein, it has a hydroxyl group and an amide group in the para position of the benzene ring. These two functional groups are highly conjugated molecules known as an auxochrome. During the photocatalysis the main contribution was reverted to both the electron-donating group –OH and the electron with drawing group $–NO_2$. Fortunately, the faster rate of degradation compared to others is assumed due to the charge attraction between negatively charged paracetamol molecules (weak acid with phenol function group; pK_a9.5) and positively charged TiO_2 NPs ameliorated the electrostatic coupling of paracetamol molecules. This, in turn, accelerated the photoreduction and the photocatalytic free-radical bombarding and cleavage.

3.2.2. Photocatalytic degradation of methylene blue (MB)

UV–Vis was employed to enable a study about the rate and degree of MB degradation (Fig. 5). The as-synthesized nanophotocatalyst was studied for seven displayed cycles. After each cycle, TiO_2@ Fe_3O_4@C–NF was simply collected by applying an appropriated external magnetic field and washed thoroughly several times then eventually recycled for another use. The kinetic plot (ln (C_x/C_0)) as a function of irradiation time was sketched for different 7 cycles, the represented fitted straight line was plotted with a slope equaled to the apparent pseudo-first-order rate constant k (min^{-1}) (Fig. 5B). The correlation constants were closed to unity and this indicates that the degradation process followed pseudo-first-order kinetics as well as Langmuir–Hinshelwood model. The photodegradation of MB was completely attained, for all fulfilled cycles, within 10 min. The photocatalyst rate of deposition K (min^{-1}) recorded equal value for Cycle 1–5, however, it confronted a slight reduction for Cycles 6 and 7.

3.3. Magnetic solid-phase extraction of ibuprofen

3.3.1. pH effect

The pH value of the sample solution has a significant influence on the adsorption of analyte molecules depending on their surface charge. NSAIDs extraction characteristics are affiliated with pH value. Whereby, NSAIDs are acidic, polar compounds including carboxylic groups, therefore, they can be found in various samples either neutral form or ionic form. If the pH value of the solution is below pKa value, these compounds turn into molecular forms. The adsorption efficiency was assumed to increase via effective intermolecular interactions between the molecular form of analyte and adsorbent. The influence of pH of sample solution on adsorption efficiency of analytes was investigated in a range of 2.0–10.0 by model solutions including 0.5 μg mL^{-1} ibuprofen. The results are shown in Fig. 6A, where, above pH 4.0, the adsorption recovery was decreased with the increase of pH values. This reduction maybe due to the weakened molecular interactions owing to the analyte ionic form escort above pH 4.0 values. The maximum adsorption recovery was obtained at pH 4.0, therefore the optimum pH 4.0 was determined for further experiments.

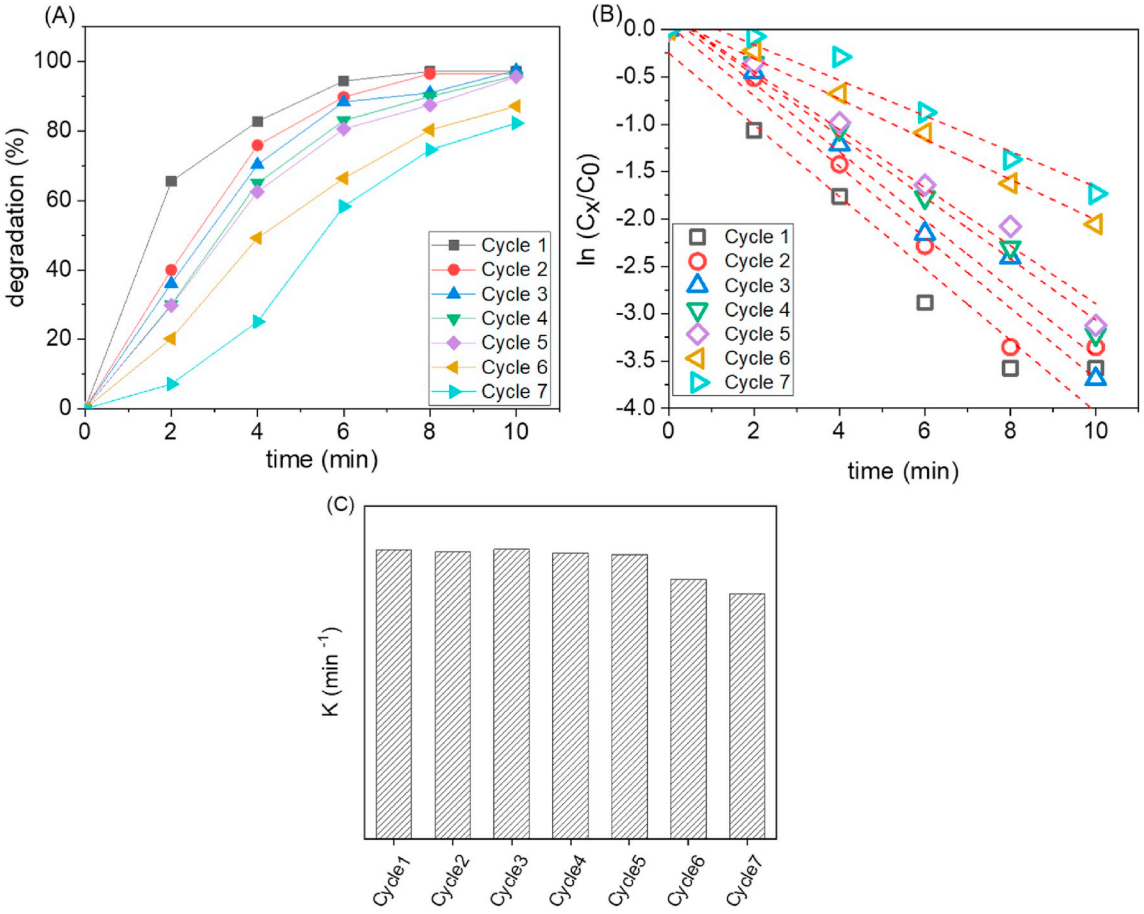

Fig. 5. (A) The degradation (%) of MB (B) The kinetic plot (ln C_x/C_0) of the photocatalytic decolorization rate of MB and (C) Pseudo-first-order rate constant k (min^{-1}) values for different reusability cycles for MB. The concentration of the photocatalyst is 0.67 mg mL^{-1}.

3.3.2. *Effect of TiO_2@Fe_3O_4@C–NF amount*

The effect of TiO_2@Fe_3O_4@C–NF amount on adsorption efficiency of Ibuprofen was investigated the range of 30–150 mg. The results are illustrated in Fig. 6B, where the adsorption recovery was increased by according to the increase of the adsorbent per unit mass. The extraction efficiency of the method was not effective until reaching a photocatalyst of mass value 150 mg. This may be attributed to the available surface interaction acquired with analytes by increasing the amount of adsorbent, thus 150 mg of TiO_2@Fe_3O_4@C–NF was used in subsequent experiments.

3.3.3. *Desorption conditions*

Initially, 150 mg adsorbent was distributed equally using Eppendorf centrifuge tubes. A model solution (15 mL) containing 0.5 μg mL^{-1} of ibuprofen was transferred to be centrifuged and the pH was adjusted to 4.0 using PBS (10 mM pH 4.0). The mixture was vortexed for 5 min for efficient adsorption of ibuprofen on TiO_2@Fe_3O_4@C-NFs. Afterwards, phase separation was carried out using an external magnet. For the elution of ibuprofen from the adsorbent surface, 5.0 mL of different organic solvents; methanol, acetonitrile, isopropyl alcohol, acetone or ethanol was added to the model solution and vortexed for 5 min. After phase separation by enabling an external magnetic field, the ibuprofen concentration of eluate was analyzed employing HPLC-DAD. From findings, it was shown that the analyte molecules could not be completely desorbed when solvents such as methanol, acetonitrile, isopropyl alcohol or ethanol were used. However, onlyacetone was able to achieve the desorption of the ibuprofen molecules on the surface of TiO_2@Fe_3O_4@C-NFs (Fig. 6C). Hence, acetone was selected as eluent for further investigations. Additionally, the effect of the volume of eluent on the efficiency of recovery was examined in the range of 1.0–5.0 mL of acetone. It was found that of acetone (2.0 mL) was adequate for the quantitative recovery of ibuprofen.

3.3.4. *Effect of sample volume*

In order to evaluate the capability of the developed method; the highest volume of the samples should be determined. Therein, it would be able to obtain a high preconcentration factor and to analyze the lowest possible analyte concentration. The effect of sample volume on the extraction efficiency of ibuprofen on the TiO_2@Fe_3O_4@C–NF was investigated in the range of 10–100 mL. As a result, the displayed method was applicable for 100 mL of the sample solution (Fig. 6D). Therefore, capacity of 100 mL of surface water collected samples with a high preconcentration factor that was able to be examined.

3.3.5. *Analytical performance parameters*

The ICH bioanalytical method validation guidelines were used to validate the TiO_2@Fe_3O_4@C-NFs-based MSPE method by considering the limit of detection (LOD), the limit of quantification (LOQ) and both intra and inter-day accuracy precision. All calibration curves were generated by graphing peak areas obtained by HPLC-DAD analysis after applying the developed MSPE method for model solutions containing a high concentration of ibuprofen. The values of the analytical performance parameters of the TiO_2@Fe_3O_4@C-NFs-based MSPE method are shown in Table 1.

Comparision of analytical performance parameters of the developed MSPE method for ibuprofen with other techniques in literature is shown in Supplementary Table S2. Our method shows better or compatible LOD, PF and RSD values than literature studies [38–45].

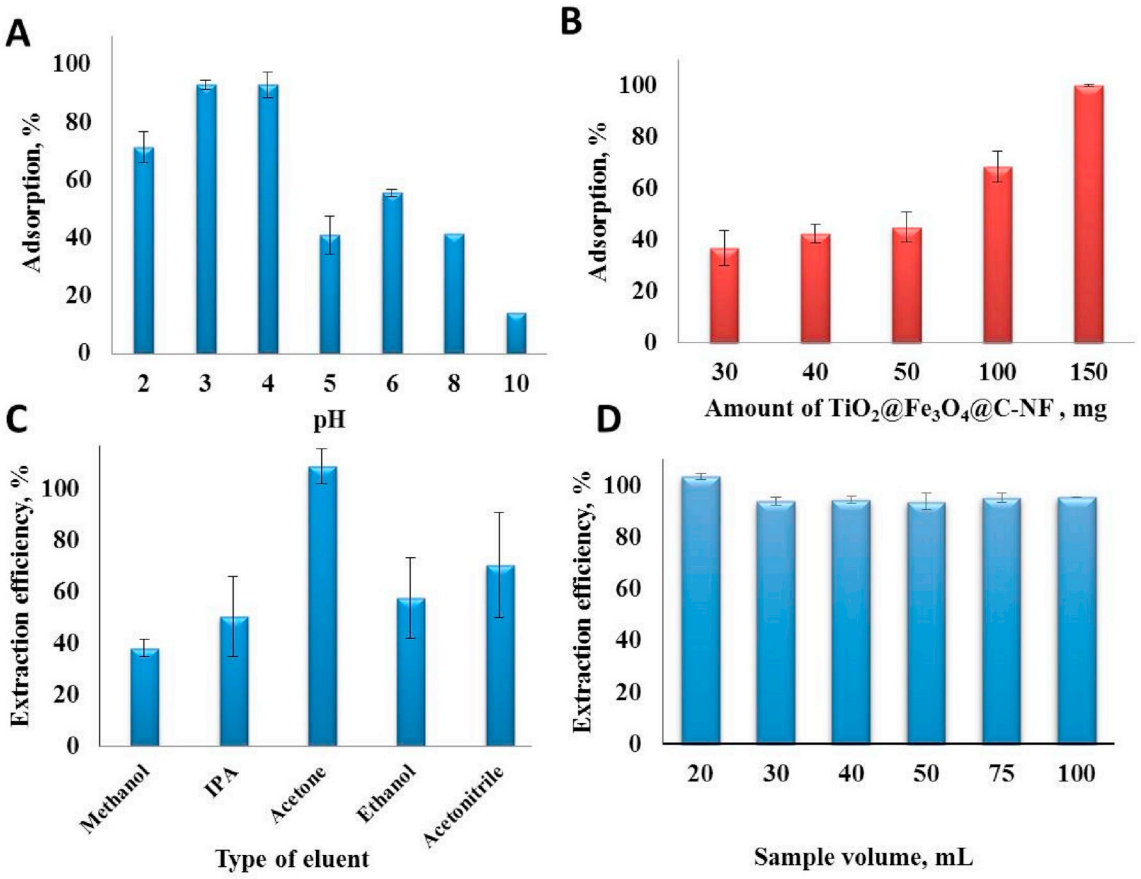

Fig. 6. Effect of different parameters on the extraction efficiency of ibuprofen (A) samples pH (B) amount of TiO_2@Fe_3O_4@C-NFs (C) type of eluent (D) samples volume. (The standard condition of samples used were: Ibuprofen concentration: 500 $\mu g{\cdot}L^{-1}$, pH:4.0, amount of TiO_2@Fe_3O_4@C-NFs: 150 mg, eluent volume: 5.0 mL, vortex mixing: 5 min, N = 3).

Table 1
The analytical performance parameter values of the TiO_2@Fe_3O_4@C-NFs-based MSPE method.

Analytical performance parameter	Value
Calibration curve equation	y = 35.055x + 15.223
R^2	0.9974
Preconcentration factor	50
LOD, $\mu g{\cdot}L^{-1}$	0.95
LOQ, $\mu g{\cdot}L^{-1}$	2.89
Intra-day precision, RSD %	1.37
İnter-day precision, RSD %	2.77
Mean Recovery, %	95

3.3.6. Application of the MSPE method to real samples for accuracy

The applicability of the described method was implemented in order to determine ibuprofen in collected environmental water, urine and pharmaceutical samples. These samples were prepared for the MSPE-HPLC-DAD procedure that was previously explained in section 2.6. The different amounts of ibuprofen were spiked into these samples given in Table 2 and these samples were subjected to the MSPE-HPLC-DAD procedure. The recoveries were in the ranges of 89–105%. Three replicate analyses of each sample was examined and the mean value was calculated. From the findings; for all examined samples, it was perceived that high level of accuracy was illustrated with a good agreement between what has been measured and the known concentration of ibuprofen inserted to the samples. The obtained results proved that the MSPE method based on TiO_2@Fe_3O_4@C–NF nanocomposite was applicable for accurate analysis of ibuprofen traces in a wide range of different matrix media.

Table 2
Analytical results of ibuprofen in pharmaceutical, biological and environmental water samples (mean ± s.d., BDL= Below the detection limit, N = 3).

Sample	Spiked amount of ibuprofen, μg	Found amount of ibuprofen, μg	Recovery, %
Pharmaceutical syrup	0	33 ± 6	–
	20	54 ± 1	105
	40	70.4 ± 1	93
Pharmaceutical tablet	0	36 ± 1	–
	30	64 ± 1	91
Sample	**Spiked amount of ibuprofen, $\mu g{\cdot}L^{-1}$**	**Found amount of ibuprofen, $\mu g{\cdot}L^{-1}$**	**Recovery, %**
Urine	0	BDL	–
	15	15 ± 0.5	100
	30	29 ± 1	97
Sea water	0	BDL	–
	250	230 ± 3	92
	500	445 ± 19	89
Waste water	0	BDL	–
	200	192 ± 4	96
	400	366 ± 16	92
Lake water	0	BDL	–
	150	153 ± 12	102
	300	293 ± 3	97

4. Conclusions

In this study, TiO_2 nanoparticles and C-nanofibers modified magnetic Fe_3O_4 nanospheres (TiO_2@Fe_3O_4@C–NF) were synthesized by using a simple hydrothermal synthesis method. This innovative

material was used as a multifunctional magnetic sorbent that exploited in the development of the magnetic solid-phase extraction method for the preconcentration of ibuprofen; and additionally as a photocatalyst for photocatalytic degradation of antibiotics, non-steroidal anti-inflammatory drugs and azo dye. It was deduced that TiO_2@Fe_3O_4@C-NFs capable to be employed for at least 15 times without losing its efficiency in the magnetic solid-phase extraction of ibuprofen. Moreover, it can be utilized, at least seven successive cycles, for the photocatalytic elimination of hazardous organic pollutants without much change in performance. The photocatalytic degradation efficiency of the TiO_2@Fe_3O_4@C–NF hybrid material for probe-analytes was between 80% and 100% overtime ranged between 8 and 125 min. This study dived slightly deeper into some environmentally required studies such as simultaneous analysis and undesired organic pollutants eliminations for collected environmental samples.

Declaration of competing interest

The authors declare no conflicts of interest.

Acknowledgments

This work has been supported by Erciyes University Scientific Research Projects Coordination Unit with research project FBA-2018-7761, Turkey.

Appendix A. Supplementary data

Supplementary data to this article can be found online at https://doi.org/10.1016/j.talanta.2020.120813.

References

[1] M. Buyukada, Removal, potential reaction pathways, and overall cost analysis of various pollution parameters and toxic odor compounds from the effluents of Turkey processing plant using TiO_2–assisted UV/O_3 process, J.Environ.Manage. 248 (2019) 109298.
[2] J. Karpińska, U. Kotowska, Removal of organic pollution in the water environment, Water 11 (2019) 2017.
[3] M. Chen, P. Wu, Z. Huang, J. Liu, Y. Li, N. Zhu, Y. Bi, Application of MgMn-layered double oxide for simultaneous efficient removal of Environmental tetracycline and Cd pollution: performance and mechanism, J. Environ. Manag. 246 (2019) 164–173.
[4] Z. Lu, W. Sun, C. Li, X. Ao, C. Yang, S. Li, Bioremoval of non-steroidal anti-inflammatory drugs by Pseudoxanthomonas sp. DIN-3 isolated from biological activated carbon process, Water Res. 161 (2019) 459–472.
[5] X. Gao, J. Geng, Y. Du, S. Li, G. Wu, Y. Fu, H. Ren, Comparative study of the toxicity between three non-steroidal anti-inflammatory drugs and their UV/$Na_2S_2O_8$ degradation products on Cyprinus carpio, Sci. Rep-UK 8 (1) (2018) 13512.
[6] M.A. Ragab, M.H. Abdel-Hay, H.M. Ahmed, S.M. Mohyeldin, Application of capillary zone electrophoresis coupled with a diode array detector (CZE-DAD) for simultaneous analysis of ibuprofen and phenylephrine, J. AOAC Int. 102 (2) (2019) 473–479.
[7] G. Sarp, E. Yilmaz, A flower-like hybrid material composed of Fe_3O_4, graphene oxide and CdSe nanodots for magnetic solid phase extraction of ibuprofen prior to its quantification by HPLC detection, Microchim. Acta 186 (11) (2019) 744.
[8] P. Aitken, I. Stanescu, R. Playne, J. Zhang, C.M. Frampton, H.C. Atkinson, An integrated safety analysis of combined acetaminophen and ibuprofen (Maxigesic®/Combogesic®) in adults, J. Pain Res. 12 (2019) 621.
[9] R.D. Oparin, M.G. Kiselev, Application of chemometrics approaches to analysis of mid-ınfrared spectra of ıbuprofen diluted in supercritical carbon dioxide, Appl. Spectrosc. 72 (10) (2018) 1548–1560.
[10] Y. Song, T. Chai, Z. Yin, X. Zhang, W. Zhang, Y. Qian, J. Qiu, Stereoselective effects of ibuprofen in adult zebrafish (Danio rerio) using UPLC-TOF/MS-based metabolomics, Environ. Pollut. 241 (2018) 730–739.
[11] E. Waraksa, M.K. Woźniak, L. Banaszkiewicz, E. Kłodzińska, M. Ozimek, R. Wrzesień, J. Namieśnik, Quantification of unconjugated and total ibuprofen and its metabolites in equine urine samples by gas chromatography-tandem mass spectrometry: application to the excretion study, Microchem. J. 150 (2019) 104129.
[12] R. Hamoudová, M. Pospíšilová, Determination of ibuprofen and flurbiprofen in pharmaceuticals by capillary zone electrophoresis, J. Pharmaceut. Biomed. 41 (4) (2006) 1463–1467.
[13] Y.A. Salem, M.E. Hammouda, M.A.A. El-Enin, S.M. El-Ashry, Application of derivative emission fluorescence spectroscopy for determination of ibuprofen and phenylephrine simultaneously in tablets and biological fluids, Spectrochim. Acta 210 (2019) 387–397.
[14] B. Mekassa, M. Tessema, B.S. Chandravanshi, M. Tefera, Square wave voltammetric determination of ibuprofen at poly (L-aspartic acid) modified glassy carbon electrode, IEEE Sensor. J. 18 (1) (2017) 37–44.
[15] N.P. Ngubane, D. Naicker, S. Ncube, L. Chimuka, L.M. Madikizela, Determination of naproxen, diclofenac and ibuprofen in Umgeni estuary and seawater: a case of northern Durban in KwaZulu–Natal Province of South Africa, Regional Studies in Marine Science 29 (2019) 100675.
[16] E. Waraksa, M. Wójtowicz-Zawadka, D. Kwiatkowska, A. Jarek, A. Małkowska, R. Wrzesień, J. Namieśnik, Simultaneous determination of ibuprofen and its metabolites in complex equine urine matrices by GC-EI-MS in excretion study in view of doping control, J. Pharmaceut. Biomed. 152 (2018) 279–288.
[17] Y. Picó, R. Alvarez-Ruiz, L. Wijaya, A. Alfarhan, M. Alyemeni, D. Barceló, Analysis of ibuprofen and its main metabolites in roots, shoots, and seeds of cowpea (Vigna unguiculata L. Walp) using liquid chromatography-quadrupole time-of-flight mass spectrometry: uptake, metabolism, and translocation, Anal. Bioanal. Chem. 410 (3) (2018) 1163–1176.
[18] R. Rodríguez-Ramos, B. Socas-Rodríguez, A. Santana-Mayor, M.A. Rodríguez-Delgado, Nanomaterials as alternative dispersants for the multiresidue analysis of phthalates in soil samples using matrix solid phase dispersion prior to ultra-high performance liquid chromatography tandem mass spectrometry, Chemosphere 236 (2019) 124377.
[19] Y. Zhang, G. Li, D. Wu, X. Li, Y. Yu, P. Luo, Y. Wu, Recent advances in emerging nanomaterials based food sample pretreatment methods for food safety screening, Trac. Trends Anal. Chem. 121 (2019) 115669.
[20] W. Jin, T. Zhou, G. Li, Recent advances of modern sample preparation techniques for traditional Chinese medicines, J. Chromatogr. A 1606 (2019) 460377.
[21] P.F. Guo, X.M. Wang, X.W. Chen, T. Yang, M.L. Chen, J.H. Wang, Nanostructures serve as adsorbents for the selective separation/enrichment of proteins, Trac. Trends Anal. Chem. 120 (2019) 115650.
[22] C.S. Jon, L.Y. Meng, D. Li, Recent review on carbon nanomaterials functionalized with ionic liquids in sample pretreatment application, Trac. Trends Anal. Chem. 120 (2019) 115641.
[23] E.V.S. Maciel, A.L. de Toffoli, E.S. Neto, C.E.D. Nazario, F.M. Lanças, F M, New materials in sample preparation: recent advances and future trends, Trac. Trends Anal. Chem. 119 (2019) 115633.
[24] M.W. Lekota, K.M. Dimpe, P.N. Nomngongo, MgO-ZnO/carbon nanofiber nanocomposite as an adsorbent for ultrasound-assisted dispersive solid-phase microextraction of carbamazepine from wastewater prior to high-performance liquid chromatographic detection, Journal of Analytical Science and Technology 10 (1) (2019) 25–36.
[25] T.G. Chatzimitakos, J.L. Anderson, C.D. Stalikas, Matrix solid-phase dispersion based on magnetic ionic liquids: an alternative sample preparation approach for the extraction of pesticides from vegetables, J. Chromatogr. A1581 (2018) 168–172.
[26] A. Khalil, W.S. Nasser, T.A. Osman, M.S. Toprak, M. Muhammed, A. Uheida, Surface modified of polyacrylonitrile nanofibers by TiO_2/MWCNT for photodegradation of organic dyes and pharmaceutical drugs under visible light irradiation, Environ. Res. 179 (2019) 108788.
[27] Z. Khani, D. Schieppati, C.L. Bianchi, D.C. Boffito, The sonophotocatalytic degradation of pharmaceuticals in water by MnOx-TiO_2systems with tuned band-gaps, Catalysts 9 (11) (2019) 949–963.
[28] N. Malesic-Eleftheriadou, E.N. Evgenidou, G.Z. Kyzas, D.N. Bikiaris, D.A. Lambropoulou, Removal of antibiotics in aqueous media by using new synthesized bio-based poly (ethylene terephthalate)-TiO_2 photocatalysts, Chemosphere 234 (2019) 746–755.
[29] A.S. Mestre, A.P. Carvalho, Photocatalytic degradation of pharmaceuticals carbamazepine, diclofenac, and sulfamethoxazole by semiconductor and carbon materials: a review, Molecules 24 (20) (2019) 3702.
[30] N. Arsalani, Y. Panahian, R. Nasiri, Fabrication of novel magnetic F-TiO2 (B)/carbon nanostructures nanocomposites as photocatalysts for malachite green degradation under visible light, Mater. Sci. Eng. B-Adv. 251 (2019) 114448.
[31] H.H. Mungondori, S. Ramujana, D.M. Katwire, R.T. Taziwa, Synthesis of a novel visible light responsive γ-Fe_2O_3/SiO_2/C-TiO_2 magnetic nanocomposite for water treatment, Water Sci. Technol. 78 (12) (2018) 2500–2510.
[32] X. Lu, Y. Li, W. Jiang, Y. Huang, W. Zhang, G. Liang, S. Yang, Porous γ-Fe_2O_3 microspheres decorated with TiO_2 nanocrystals as highly recyclable photocatalysts and potential highly efficient magnetic hyperthermia agents, J. Mater. Sci. Mater. Electron. 29 (24) (2018) 20856–20865.
[33] S. Da Dalt, A.K. Alves, C.P. Bergmann, Preparation and performance of TiO_2-ZnO/CNT hetero-nanostructures applied to photodegradation of organic dye, Mater. Res. 19 (6) (2016) 1372–1375.
[34] L. Stagi, C.M. Carbonaro, R. Corpino, D. Chiriu, P.C. Ricci, Light induced TiO_2 phase transformation: correlation with luminescent surface defects, Phys. Status Solidi B 252 (1) (2015) 124–129.
[35] H. Cottin, M.C. Gazeau, J.F. Doussin, F. Raulin, An experimental study of the photodegradation of polyoxymethylene at 122, 147 and 193 nm, J. PhotochPhotobio A135 (1) (2000) 53–64.
[36] S. Monti, S. Sortino, G. De Guidi, G. Marconi, Photochemistry of 2-(3-benzoylphenyl) propionic acid (ketoprofen) Part 1A picosecond and nanosecond time resolved study in aqueous solution, J. Chem. Soc., Faraday Trans. (13) (1997) 2269–2275.
[37] K. Zessel, S. Mohring, G. Hamscher, M. Kietzmann, J. Stahl, Biocompatibility and antibacterial activity of photolytic products of sulfonamides, Chemosphere (2014) 167–174.
[38] A. Beiraghi, K. Pourghazi, M. Amoli-Diva, Mixed supramolecular hemimicelles

aggregates and magnetic carrier technology for solid phase extraction of ibuprofen in environmental samples prior to its HPLC-UV determination, Chem. Eng. Sci. 108 (2014) 103–110, https://doi.org/10.1016/j.ces.2013.12.044.
[39] M. Locatelli, V. Ferrone, R. Cifelli, R.C. Barbacane, G. Carlucci, Microextraction by packed sorbent and high performance liquid chromatography determination of seven non-steroidal anti-inflammatory drugs in human plasma and urine, J. Chromatogr., A 1367 (2014) 1–8, https://doi.org/10.1016/j.chroma.2014.09.034.
[40] M.R. Payán, M.Á.B. López, R. Fernández-Torres, M.V.N. Manuel, C. Mochón, Hollow fiber-based liquid-phase microextraction (HF-LPME) of ibuprofen followed by FIA-chemiluminescence determination using the acidic permanganate–sulfite system, Talanta 79 (2009) 911–915.
[41] V. Manzo, L. Honda, O. Navarro, L. Ascar, P. Richter, Microextraction of non-steroidal anti-inflammatory drugs from waste water samples by rotating-disk sorptive extraction, Talanta 128 (2014) 486–492.
[42] D. Yuvali, I. Narin, M. Soylak, E. Yilmaz, Green synthesis of magnetic carbon nanodot/graphene oxide hybrid material (Fe3O4@C-nanodot@GO) for magnetic solid phase extraction of ibuprofen in human blood samples prior to HPLC-DAD determination, J. Pharmaceut. Biomed. Anal. 179 (2020) 113001.
[43] M.R. Payán, M.Á.B. López, R. Fernández-Torres, J.L.P. Bernal, M.C. Mochón, HPLC determination of ibuprofen, diclofenac and salicylic acid using hollow fiber-based liquid phase microextraction (HF-LPME), Anal. Chim. Acta 653 (2009) 184–190.
[44] N.N. AL-Hashimi, H.A. Aleih, I.I. Fasfous, H.S. AlKhatib, Multi-walled carbon nanotubes as efficient sorbent for the solid bar microextraction of non-steroidal anti-inflammatory drugs from human urine samples, Curr. Pharmaceut. Anal. 14 (2018) 239–246.
[45] A. Kretschmer, M. Giera, M. Wijtmans, L. de Vries, H. Lingeman, H. Irth, W.M.A. Niessen, Derivatization of carboxylic acids with 4-APEBA for detection by positive-ion LC-ESI–MS(/MS) applied for the analysis of prostanoids and NSAID in urine, J. Chromatogr. B 879 (2011) 1393–1401.